Hindawi
Geofluids
Volume 2022, Article ID 3262350, 13 pages
https://doi.org/10.1155/2022/3262350

Research Article

Investigation of Anisotropic Behavior and Statistical Evolution of Acoustic Emission Energy during the Deformation of Layered Sandstone

Shujian Li,[1,2,3] **Shaobin Dong**,[1] **Binting Cai**,[1] **Menglai Wang**,[1,2] **Yanhong Xie**,[1] **and Jingguo Luo**[1]

[1]*Yunnan Phosphate Chemical Group Co., Ltd., Kunming Yunnan 650600, China*
[2]*National Engineering and Technology Research Center for Development and Utilization of Phosphate Resources, Kunming Yunnan 650600, China*
[3]*State Key Laboratory of Coal Mine Disaster Dynamics and Control, Chongqing University, Chongqing 400044, China*

Correspondence should be addressed to Shujian Li; lishujiancqu@163.com

Received 1 April 2022; Revised 15 May 2022; Accepted 26 May 2022; Published 28 June 2022

Academic Editor: Hao Wu

To further understand the anisotropic behavior of layered rock and the precursor characteristics of rock mass instability, a series of uniaxial compression experiments using a loading system and an acoustic emission system was conducted on sandstone specimens. The influence of bedding on the mechanical parameters and failure modes and the statistical evolution of the acoustic emission energy were successively discussed. The results of axial stress-strain curves and crack propagation modes showed that the existence of a bedding plane increased the anisotropy of the rocks, and the magnitude of the bedding inclination also exerted certain influence on this anisotropy. Furthermore, we used the least squares method and the maximum likelihood method to analyze the b value and power-law exponent, respectively. The results of statistical evolution of acoustic emission energy showed that the b value, the effective power-law exponent, and the optimal exponent could be used as monitoring indexes for the rock mass stability. With the progress of the experiment, the following phenomena pertaining to acoustic emission activities occurred, which may indicate imminent danger of collapse: (1) the crackling noises increased significantly; (2) the variation of the b value exhibited a significant downward trend; and (3) the effective power-law exponent and the optimal exponent changed in different stages and gradually decreased as the final failure was approached. The findings in this paper may provide a theoretical basis for predicting the collapse and instability of rock mass structures.

1. Introduction

With the exploitation and utilization of deep underground solid mineral resources, the phenomena of collapse and instability of rock mass structures have become increasingly conspicuous. For example, the failure of rock pillars under the gravity of the roof has led to collapse accidents [1], and the fracture of an aquifuge under the action of water pressure has resulted in a mine flood accident [2]. Furthermore, a rock usually contains some bedding planes inclined in a certain direction (Figure 1), which indicates rock anisotropy and increases the difficulty of deformation analysis of rock masses [3–6]. Therefore, further understanding the anisotropic behavior of layered rock and the precursor characteristics of rock mass instability is of considerable significance to predict the collapse and instability of rock mass structures.

In this paper, the bedding inclination (β) of layered rock is defined as the angle between the bedding plane and horizontal direction, as shown in Figure 1. In a large number of studies on layered rock, most scholars focused primarily on the anisotropic behavior in terms of the strength and fracture pattern [7–12]. For example, Yin and Yang [7] analyzed the characteristics of

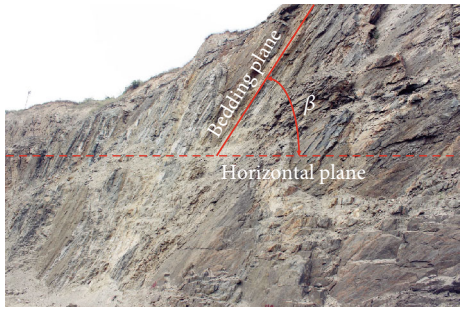

Figure 1: Diagram of layered rock mass.

layered sandstone under uniaxial compression and Brazilian testing. In their study, the uniaxial compression strength and the Brazilian tensile strength decreased overall with increase in the bedding inclination. Furthermore, by adopting 3D digital image correlation system and strain gauges, the authors analyzed the deformation and failure mechanism of the specimens. He and Afolagboye [8] studied the effects of the bedding inclination and interlayer bonding force on the mechanical behavior of inherently anisotropic shale rocks. The authors found that decrease in the interlayer bonding force resulted in increase in the anisotropic behavior. Khanlari et al. [9] investigated the fracture behavior of laminated sandstones under Brazilian tests and categorized the fracture mode of the specimens into two types: (1) failure mode that is a function of laminations and (2) failure mode independent of laminations. However, there are few articles describing the anisotropic behavior of rocks from the perspective of monitoring and warning for rock mass failure.

Furthermore, with the development of science and technology, novel testing techniques have been used to study the fracture characteristics of rocks, such as the use of scanning electron microscopes (SEM) [13], 3D-printing technology [14], computerized tomography (CT) [15], and acoustic emission (AE) monitoring technology [16–18]. The failure process of rock demonstrates a self-organized critical behavior [19, 20]: a large number of microfractures (avalanches) are generated from disordered distribution to centralized distribution, which eventually leads to macrocrack propagation until rock failure occurs. Each microfracture event (avalanche event) is accompanied by an equivalent acoustic emission signal, which can be detected by acoustic emission experiments. Therefore, the acoustic emission monitoring technology is widely used in the field of rock engineering. In terms of layered rock, the acoustic emission monitoring technology is mainly used to analyze the anisotropic characteristics of acoustic emission parameters [21], the relationship between the acoustic emission parameters and stress [22], and the relationship between the acoustic emission parameters and fracture mode [23]. In addition, some scholars adopted the Gutenberg-Richter relationship to analyze the statistical characteristics of acoustic emission parameters during the rock fracture process [24–27]; however, only a few similar studies exist for layered rocks, especially in terms of the statistical evolution of the acoustic emission energy of layered rocks.

Therefore, to further understand the anisotropic behavior and the stability problem of rock pillars and rock strata, we conducted a series of uniaxial compression tests on layered and intact sandstone samples and further analyzed the influence of bedding on the mechanical parameters and failure modes of selected samples. At the same time, the acoustic emission monitoring technology was used to determine the acoustic emission energy released during the deformation of selected samples. According to the theory of statistics, the statistical evolution of acoustic emission energy was discussed by using the least squares method and the maximum likelihood method, which provided a theoretical basis for disaster prediction.

2. Specimen Preparation and Testing

2.1. Specimen Preparation. Sandstone is a granular material occurring commonly in nature, and its main mineral components are quartz and feldspar. In this study, sandstone samples were obtained from a mine in Chongqing City, China. After a blasting operation was carried out on the site of the heading face, we selected the bedding blocks with no macrocracking in the same location. In addition, some intact blocks without bedding planes were selected to produce intact specimens, which were used to compare the anisotropy of layered rocks. By coring, cutting, and grinding in the laboratory, we obtained two types of sandstone specimens with bedding inclination and one group of intact specimens. According to the testing guidelines specified by the International Society for Rock Mechanics (ISRM), the ends of the specimens were ground flat by a double-face grinding machine to within ±0.02 mm. All tested sandstone specimens were made into cylinders with a height of 100 mm and diameter of 50 mm. The bedding inclinations (β) of the layered rock were approximately 20° and 80°. The sample number was defined as the "sample type-test number." Here, A, B, and C represent the intact specimen, the specimen with a bedding inclination of approximately 20°, and the specimen with a bedding inclination of approximately 80°, respectively. For example, "B-2" represents a specimen with a bedding inclination of approximately 20° being tested for the second time. Figure 2 shows the material objects and related parameters of the sandstone specimens used in this study.

2.2. Testing System. In this study, the experimental instruments mainly included a loading equipment, an acoustic emission monitoring system, and a CT scanning system. A YSSZ-500A biaxial compression creep tester was selected for the loading equipment, and its maximum load was 500 kN; the loading method was displacement control, and the loading speed was 0.1 mm/min. A PCI-2 acoustic emission monitoring system manufactured by the American Physical Acoustics Company was used to monitor the process of compression failure of the specimens, and its threshold for detection was set to 40 dB. The CT scanning system was a SOMATOM Scope X-ray spiral CT machine, which was used to reconstruct the failure modes of the specimens. The spatial resolution and scanning slice of the CT machine were 0.28 mm × 0.28 mm and 0.75 mm, respectively.

Before the test, the selected samples were dried for 24 h to reduce the influence of the water content on the rock

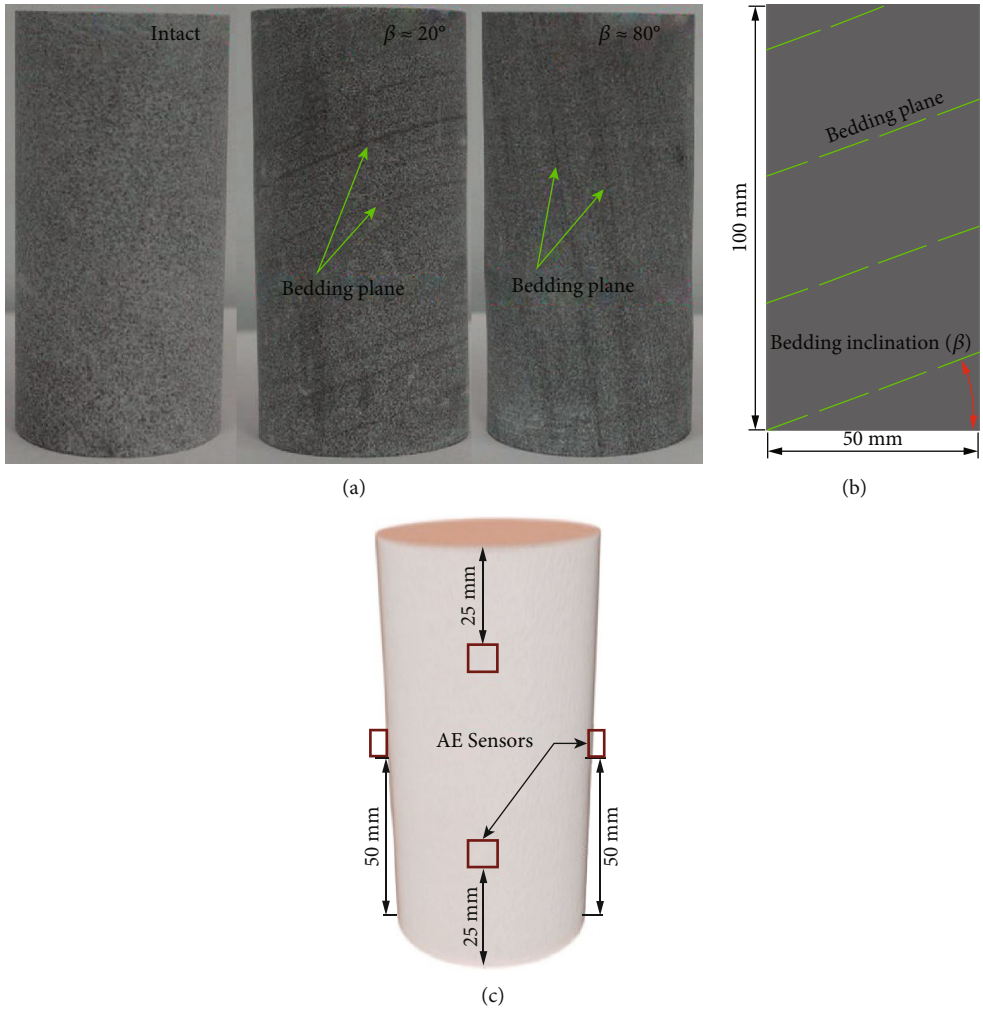

Figure 2: Diagram of selected samples: (a) material objects; (b) detailed geometries; (c) schematic of arrangement of AE sensors. The green dotted line represents the bedding plane of the specimen.

anisotropy. Four AE sensors were arranged on the surface of the specimen, and their position parameters are shown in Figure 2(c). At the same time, the ends of the specimen were coated with a layer of butter to reduce the interference of the end effect on the acoustic emission signals. The signal source was simulated by knocking the specimen with a small wooden rod before the test, which was used to ensure the normal operation of each channel probe. Moreover, the loading system and acoustic emission system were simultaneously turned on to synchronously collect the mechanical and acoustic emission parameters during compression failure of the specimen. Finally, the fracture modes of the failure specimens were observed by using the CT machine.

3. Experimental Results and Theoretical Analysis

3.1. Influence of Bedding on Mechanical Parameters. Figure 3 shows the axial stress-strain curves of the selected samples under uniaxial compression. The peak strength, peak strain, and elastic modulus of the specimens are presented in Table 1. Figure 3 indicates that the variation trends of the stress-strain curves of the intact and layered specimens are basically the same during the entire failure process, and all the specimens go through four stages: compaction, elasticity, yield, and failure. Moreover, the axial stress of the failure specimens does not decrease to zero immediately, as shown in Figure 3, which indicates that these specimens still possess a certain bearing capacity. In this study, the elastic modulus is defined as the slope of the straight segment of the stress-strain curve. By comparing and analyzing the mechanical parameters (peak strength, peak strain, and elastic modulus) of the intact and layered samples, as specified in Table 1, it can be concluded that the peak strength and elastic modulus of the layered samples are smaller than those of the intact samples. However, it should be noted that there exists a minor difference between the peak strains of the layered and intact specimens. This result may have occurred because the bedding plane was thin, the peak strain was a result of mainly the compaction of pores and microcracks, and the axial deformation caused by sliding along the bedding plane occurred mainly after the peak strength had been reached.

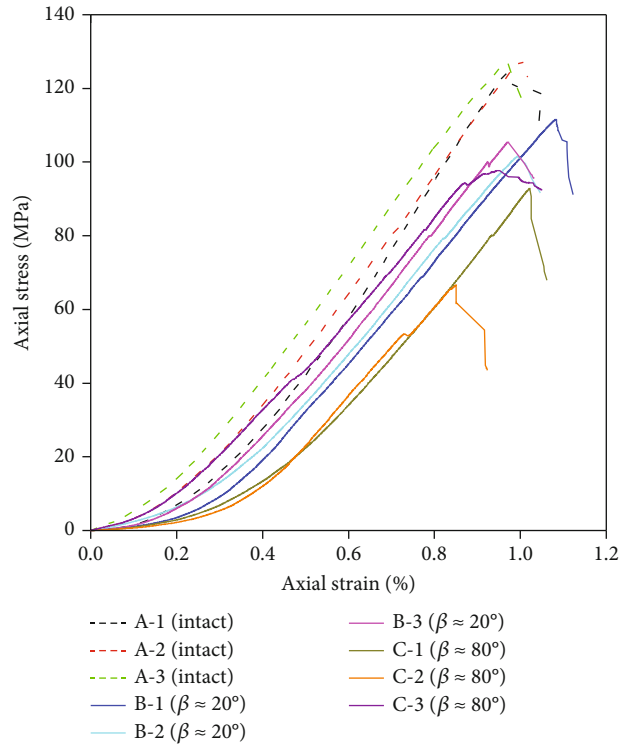

Figure 3: Axial stress-strain curves of selected samples under uniaxial compression.

Due to the limitations of field sampling, in this study, we selected only two types of layered specimens (specimen B and specimen C), which mainly analyze the difference of deformation and fracture of layered rock with slow dip angle and steep dip angle. From Table 1, it can be concluded that the peak strength and elastic modulus of specimen B are greater than those of specimen C, which indicates that it is potentially easier to destroy specimens with a large bedding inclination under a compression condition. Therefore, we inferred that shear slipping occurred more easily when the bedding inclination was larger. To verify this hypothesis, we analyzed the failure modes of the specimens, as described in the next section. In summary, the existence of bedding planes reduces the peak strength and elastic modulus of rock; however, it does not considerably influence the peak strain of the specimens. In addition, the mechanical parameters of the specimens are affected by the bedding inclination, and the strength of the specimens with a large bedding inclination is usually low under uniaxial compression.

3.2. Influence of Bedding on Failure Modes. Figure 4 shows the failure modes of the selected samples after uniaxial compression. From Figure 4, we can see that the selected samples underwent critical damage, and some rock blocks either fell off or disappeared. Therefore, it could be determined that sandstone specimens exhibit strong brittleness under uniaxial compression. Moreover, the failure mode of the specimens was primarily shear failure, as shown in Figure 4. It can be seen that failure criterion of rock under compressive load generally satisfies the Mohr-Coulomb criterion. The failure modes of the intact specimens could be generalized into two modes: single incline plane shear failure (Figure 4(a)) and X-conjugated incline plane shear failure (Figures 4(b) and 4(c)). The failure mode of specimen B included shear failure across the matrix and bedding plane (Figures 4(d)–4(f)), and one end of specimen B demonstrated the failure characteristics of a cone, which may be due to the friction between the end of specimen B and the loading head of the testing machine. Furthermore, some rock blocks at the end of specimen B detached or disappeared, which may be related to the crack propagation along the bedding planes. The failure mode of specimen C was mainly shear failure along the bedding planes (Figures 4(g)–4(i)), which indicates that the "layer activation" mode occurs at high bedding inclinations. In this study, the failure mode was considered to be a "layer activation" mode when the fracture planes were parallel to the bedding planes. Therefore, the failure modes of the selected samples were related to the bedding planes and bedding inclination, and the failure modes of the specimens with large bedding inclination were usually "layer activation" modes.

3.3. Statistical Evolution of Acoustic Emission Energy. Due to the self-organized critical behavior of rock, the phenomenon of microfracture clustering occurs before rock failure, and various precursor phenomena are gradually recognized, such as a decrease in stress and increase in crackling noises [28, 29]. Every microfracture event radiates elastic wave in the surroundings to produce AE phenomenon during the rock failure process; thus, we often use AE activities to characterize the deformation and failure characteristics of rock. The occurrence of an AE activity is accompanied by the rapid release of energy in a material, which can be detected by using acoustic emission experiments. Therefore, we used the least squares method and the maximum likelihood method to analyze the large amount of acoustic emission energy data obtained in the experiment, to determine the statistical evolution of the acoustic emission energy during the rock failure process. In this study, the acoustic emission energies were acquired by fast numerical integration of the square voltage of signals [30], as follows:

$$Q = \frac{1}{R}\int_{t_0}^{t_1} V^2(t)dt, \tag{1}$$

where b is the acoustic emission energy, b is the voltage, and b is the reference electrical resistance. b and b denote the starting and ending times of the voltage transient record, respectively.

3.3.1. Evolution Law of the b Value. Gutenberg and Richter discovered the following logarithmic relationship between the earthquake frequency and magnitude [31]:

$$\log_{10}(N) = a - bM, \tag{2}$$

where$M$ is the magnitude of the earthquake and N is the number of earthquakes with magnitudes ranging between M and $M + \Delta M$. ΔM is the length of a magnitude interval, and a and b are constants. Equation (2) is also called the Gutenberg-Richter formula (G-R relation). In the case of

Table 1: Mechanical parameters of selected samples (units: °, MPa, %, and GPa).

Specimen number	β (°)	Peak strength (MPa)		Peak strain (%)		Elastic modulus (GPa)		Specimen type
		Measured value	Mean value	Measured value	Mean value	Measured value	Mean value	
A-1	—	124.4		0.97		17.3		
A-2	—	127.4	126.3	1.00	0.98	16.2	16.6	Intact specimen
A-3	—	127.0		0.97		16.3		
B-1	20	111.5		1.08		14.2		
B-2	20	101.7	106.2	1.00	1.02	14.3	14.6	
B-3	20	105.4		0.97		15.4		Layered specimen
C-1	80	92.8		1.02		13.2		
C-2	80	66.7	85.7	0.85	0.94	13.3	13.5	
C-3	80	97.7		0.95		14.0		

the AE technique, a considerable number of studies have suggested that the relationship between the frequency and energy level for AE activity during rock failure process satisfies the Gutenberg-Richter formula, and the magnitude (M) or energy level is replaced by the AE signal amplitude [32, 33]. In this paper, we used the logarithm of the acoustic emission energy as the magnitude (M), as follows:

$$M = \log_{10}(Q). \tag{3}$$

For the fracture process of rock, the change trend of the b value can represent the scale of crack propagation and the damage degree of rock [34–37]. The increasing proportion of high-energy avalanche events leads to a decrease in the b value, and the increasing proportion of low-energy avalanche events leads to an increase in the b value. A larger range of fluctuation of the b value indicates that the crack propagation is more unstable. The formulas for calculating the b value by using the least squares method are as follows [31, 38]:

$$b' = \frac{\sum_{k=1}^{m} M_k \times \sum_{k=1}^{m} \log_{10}(N_k) - m\sum_{k=1}^{m} M_k \log_{10}(N_k)}{m\sum_{k=1}^{m} M_k^2 - \left(\sum_{k=1}^{m} M_k\right)^2}, \tag{4}$$

$$\Delta M = M_{k+1} - M_k, \tag{5}$$

where b' is the estimated b value. In this study, $[M_k - (\Delta M/2), M_k + (\Delta M/2))$ is regarded as a magnitude interval, the length of the magnitude interval is 0.1 in this study (b'), b' (b') is the median of each magnitude interval, and b' is the cumulative counts of AE signals in the magnitude interval $[M_k - (\Delta M/2), M_k + (\Delta M/2))$.

To reduce the need for repetition of the same type of data analysis, the least squares method was adopted to compare and analyze the specimens A-1, B-1, and C-1. The b' value of the selected samples was calculated in the following manner: (1) the deformation and failure time of the specimen was divided into several groups according to a time interval of 75 s, and the corresponding AE parameters of each group were obtained. When the duration time of AE activities of the last group was less than 15 s, the corresponding AE data of the last two groups were grouped into one group for calculation, which could avoid the large errors caused by the presence of insufficient AE energy data in the calculation. For example, if the deformation and failure time of the specimen was 1533 s (sample A-1), then the data were separated into 21 groups: [0,75), [75,150), [150,225), …, [1425,1500), and [1500,1575). (2) The b' value of each group could be calculated according to Equations (2)–(5). (3) The abscissa of each group without the last group was the right endpoint of the time interval, and the abscissa of the last group was the end time of the experiment. The results of the analysis of the b' value of the selected samples are shown in Figure 5 and Table 2.

Figure 5 shows the evolution of the b' value and the AE energy versus testing time for the selected samples. From Figure 5, it can be observed that the b' value curves along the time axis for the selected samples are not smooth, which may be caused by the inhomogeneous mechanical properties of the specimens and the unstable propagation of cracks. It is worth noting that the b' value curves along the time axis for layered specimens were more uneven than those of intact specimens, which indicated that the existence of the bedding plane could increase the anisotropy of rocks. Moreover, the trends in the variation of the b' value for the selected samples were basically similar, as shown in Figure 5, and the number of avalanche events in a group had little effect on the change trends of the b' values, although it exerted a notable influence on the magnitude of these values. With the progress of the uniaxial compression experiment, the b' value first decreases, fluctuates, and finally decreases again. Because the variation of the b' value of the selected samples demonstrated a decreasing trend after the corresponding moment of the b'_1 value (Figure 5), the deformation process of the specimens could be divided into two stages, and the corresponding time of b'_1 value could be considered as the turning point of the process of acoustic emission energy release.

In stage I, the b' value fluctuated within a certain range, which indicates that the low energy ($Q \le 50$ aJ) and high energy ($Q > 50$ aJ) released by avalanche events occupy dominant positions alternately (Figure 5), and the specimen starts

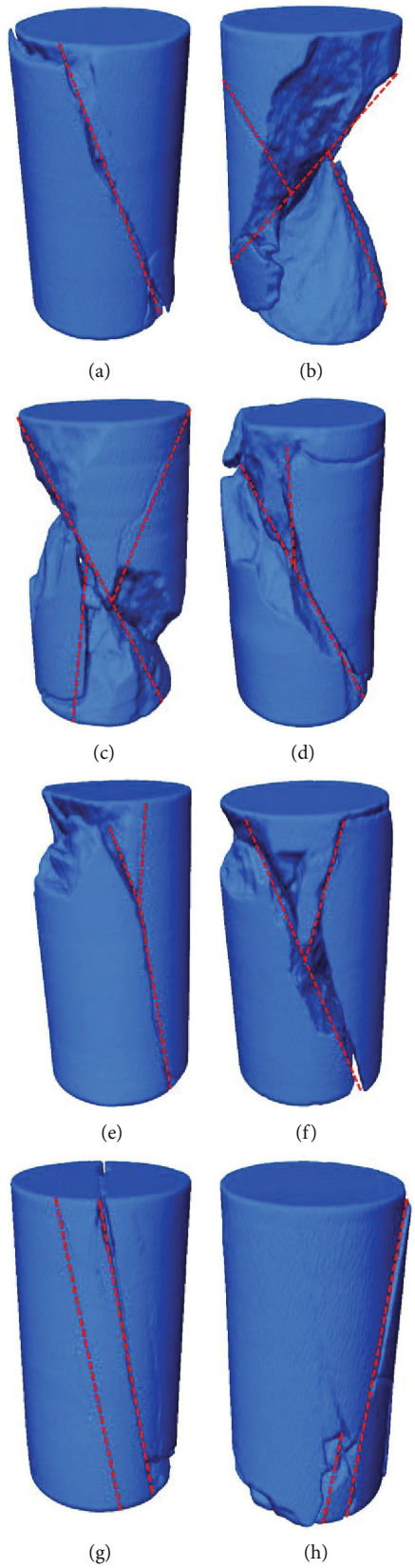

Figure 4: Continued.

(i)

Figure 4: Failure modes of selected samples after uniaxial compression: (a) A-1; (b) A-2; (c) A-3; (d) B-1; (e) B-2; (f) B-3; (g) C-1; (h) C-2; (i) C-3. The dotted line represents the approximate position of the main fracture surface of specimens.

to develop microfractures, which expand successively. According to the magnitude of the acoustic emission energy in Figure 5, it can be seen that the number of low-energy avalanche events in this stage is higher, and the number of high-energy avalanche events is lower. If the total amount of acoustic emission energy generated in this stage is little and there are few high-energy avalanche events, then the available data points for fitting the curve may be insufficient, which has a certain impact on the calculation of the b value. Compared with the intact specimen, the b' value of the layered specimen demonstrated larger fluctuations in this stage. As seen from Figure 5, this result may be due to the relatively large number and frequent occurrence of the high-energy avalanche events for the layered specimen in this stage. It is worth noting that the variation of the b' value demonstrated an upward trend in the later period of this stage; thus, it could be inferred that the microfractures increased again and began to accumulate, which indicates imminent danger of collapse.

In stage II, the variation of the b' value demonstrated a significant downward trend, and the acoustic emission energy started to increase rapidly to the peak values (Figure 5), which could be used as "early warning signals" before the occurrence of the final collapse. This result may have occurred because the macrocracks began to appear and propagate until the specimen failed. According to Table 2, the b'_1 values of the layered specimens are larger than those of intact specimens, which indicates that the number of microfracture events of the layered specimens is high; thus, it can be concluded that the damage degree of the layered specimens is larger than that of intact specimens before the beginning of the second stage. When approaching the final failure of the specimens, the range of decrease in the b' value suddenly increased, and the crackling noise also increased significantly, which indicated a significant increase in the number of higher-energy avalanche events. In this study, η is defined as the change rate of the b' value when the final failure of the specimens is approached:

$$\eta = \frac{\left|b'_3 - b'_2\right|}{b'_2} \times 100\%. \tag{6}$$

Here, a higher η value indicates that the rock is more brittle. According to Table 2, the η values of the layered specimens are smaller than those of the intact specimens. Furthermore, the maximum AE energies of the specimens A-1, B-1, and C-1, as shown in Figure 5, are 6.7×10^9 aJ, 2.1×10^5 aJ, and 2.7×10^6 aJ, respectively. Therefore, we inferred that the existence of the bedding plane could reduce the brittleness of rock. It is worth noting that the η value of specimen C-1 was larger than that of specimen B-1, but it was closer to the η value of the intact specimen, which indicates that the "layer activation" mode occurred more suddenly than other failure modes of the layered specimens.

3.3.2. Evolution Law of Power-Law Exponent. According to the study of the acoustic emission energy distribution during the rock failure process [27], another expression for the Gutenberg-Richter formula can be defined as follows:

$$P(Q)dQ \sim \frac{Q^{-r}}{Q_{\min}^{1-r}} dQ, \quad Q > Q_{\min}, \tag{7}$$

where $Q_{\min}$ is the lower cutoff needed for normalization and b is the power-law exponent. Utsu and Li et al. indicated that the relation between the values of b and b satisfied Equation (8) during the rock failure process [39, 40].

$$r = 1 + b. \tag{8}$$

Therefore, $r'(Q_{\min}) = 1 + n[\sum_{j=1}^{n} \ln(Q_j/Q_{\min})]^{-1}$ is also regarded as an important parameter to measure the variation degree of crack propagation. According to the results of the abovementioned research, we used the maximum likelihood method to estimate the power-law exponents of the acoustic emission energy distributions in two stages (stage

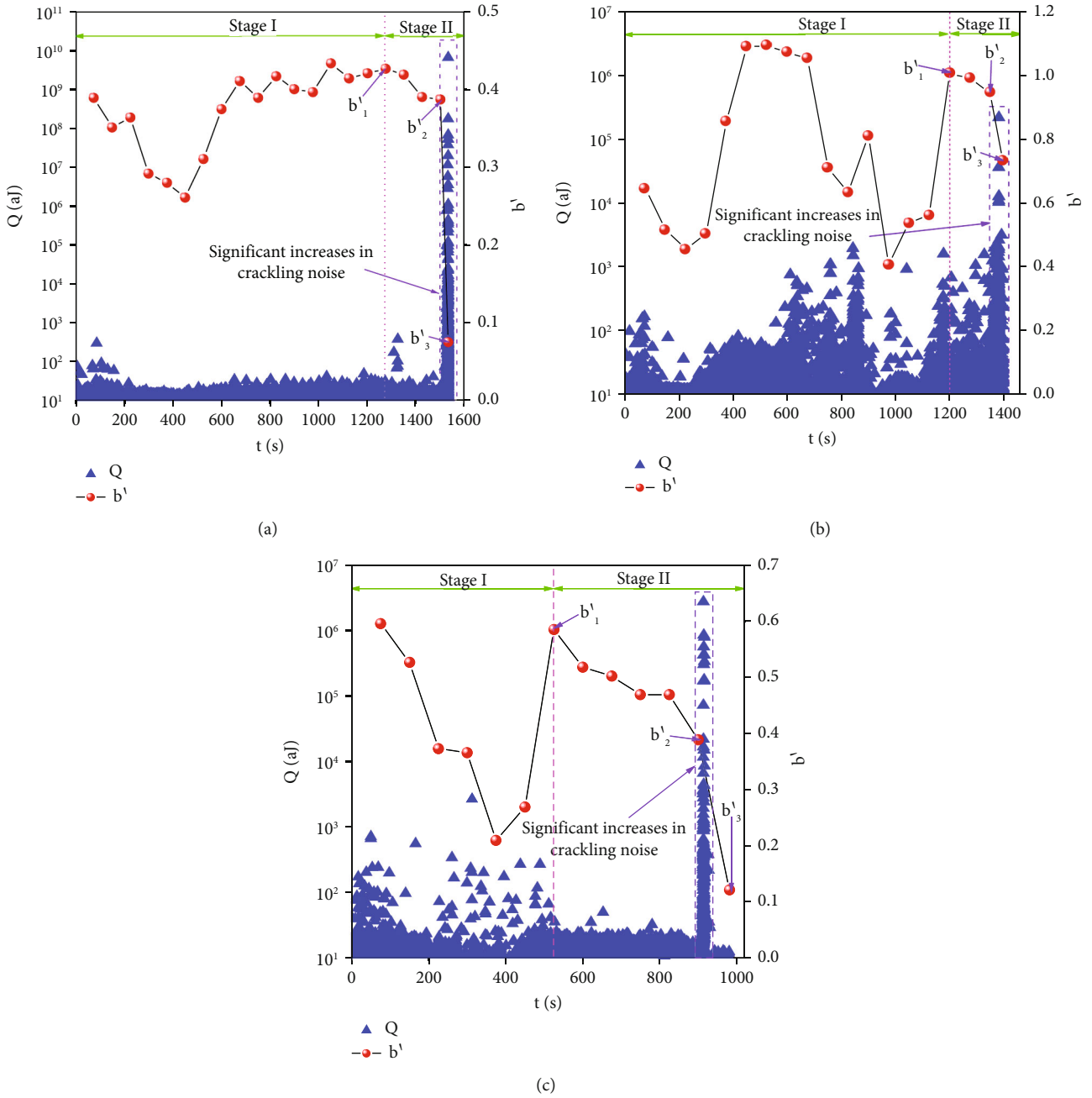

Figure 5: Estimated value of b and the acoustic emission energy versus time evolutions for the specimens: (a) A-1; (b) B-1; (c) C-1.

I and stage II) [27], as follows:

$$r'(Q_{\min}) = 1 + n\left[\sum_{j=1}^{n} \ln \frac{Q_j}{Q_{\min}}\right]^{-1}, \quad \sigma = \frac{r'(Q_{\min}) - 1}{\sqrt{n}} + O(n^{-}1), \tag{9}$$

where r', r', are the observed values of r' such that r'. r' is an estimated value of the power-law exponent, and r' is the standard error.

Figure 6 shows the r' values for the two stages during the compression failure of the specimens. In this study, the r' values of the initial shoulders of the curves in Figure 6 were considered as the effective power-law exponents. $r_1{}'$ is the effective power-law exponent of the first stage, $r_2{}'$ is the effective power-law exponent of the second stage, and $\Delta r = r_1{}' - r_2{}'$ represents the difference in the effective power-law exponents for the two stages. Moreover, the plateau of the curves in Figure 6 defines the optimal exponent (w). w_1 is the optimal exponent of the first stage, w_2 is the optimal exponent of the second stage, and $\Delta w = w_1 - w_2$ represents the difference in the optimal exponents for the two stages. While the plateau

Table 2: The b' values of selected samples (units: s, %).

Specimen	t (s)	b' value		η (%)
		Category	Value	
A-1	1275	b'_1	0.43	79.49
	1500	b'_2	0.39	
	1533	b'_3	0.08	
B-1	1200	b'_1	1.01	23.16
	1350	b'_2	0.95	
	1398	b'_3	0.73	
C-1	525	b'_1	0.58	69.23
	900	b'_2	0.39	
	982	b'_3	0.12	

is not as clean as possible, the optimal exponent can be determined from the r' value of the initial shoulder of the curve. From Figure 6, the red dotted line defines the value of the optimal exponent of the first stage, and the blue dotted line defines the value of the optimal exponent of the second stage. The exponents of the selected samples and their difference values are listed in Table 3.

The change trends of the r' value curves for the two stages of a specimen are basically the same, as shown in Figure 6, which indicates that the AE activities for the two stages of a specimen have self-similar characteristics in the statistical distribution. It is worth noting that the plateaus of the r' value curves of the first stage do not develop as well as those of the second stage, potentially because the low acoustic emission activity in the first stage leads to the generation of less acoustic emission data. For the same value of $Q_{\min}$, the r' values of the second stage are usually smaller than those of the first stage, as shown in Figure 6. By comparing and analyzing the effective power-law exponents and the optimal exponents of the selected samples and their difference values (Table 3), the Δr values and Δw values of the specimens are noted to be positive. These results indicate that the exponents of the specimens change in different stages with increasing axial stress, and the effective power-law exponents and the optimal exponents decrease as the final failure of the specimens is approached. Therefore, it was determined that the variation of the effective power-law exponents and the optimal exponents exhibits a downward trend, which can be regarded as a warning signal for the impending major collapse.

4. Discussion

The results of this paper showed that the existence of a bedding plane increases the anisotropy of rocks, and the size of the bedding inclination also influences the anisotropy of rocks [7–12, 21–23]. In terms of the mechanical parameters, the effects of the bedding plane on the peak strength, peak strain, and elastic modulus were analyzed. Generally, the strength of the specimens with a large bedding inclination was low, and the peak strength and elastic modulus of layered rocks were lower than those of intact rocks [7]. In terms of failure modes, the failure modes of rocks with a large bedding inclination were usually "layer activation" modes [9]. The analysis of the rock mechanics parameters indicated that the peak strengths of the layered rocks were generally the lowest, and the failure mode of the layered rocks was shear failure along the bedding planes [10]. As a result, rock mass sliding along the bedding plane may occur under low stress, which is extremely hazardous for human life and property. In terms of the b value, the existence of the bedding plane increased the instability of the crack propagation and reduced the brittleness of the rocks. It is worth noting that the variation of the b value exhibited a downward trend, and the acoustic emission energy began to increase rapidly to the peak values, which could be used as an "early warning signal" before the occurrence of the final collapse. The power-law exponent of the crackling noises during the rock failure process changed in different stages and gradually decreased as the final failure was approached, which was regarded as an early signal of rock mass instability [27, 29]. At the same time, the physical significances of the effective power-law exponent and the optimal exponent were introduced. Involving a comparative analysis of the experimental results presented above, our research has two major implications.

First, this paper enriched the mechanical and acoustic theories of monitoring and warning for rock mass failure. Considering the mechanical theory, the bedding plane and bedding inclination exerted considerable influence on the peak strength of the rock; however, they had a little influence on the peak strain of the rock. In terms of the acoustic theory, the statistical evolution of the crackling noise was analyzed by using the least squares method and maximum likelihood method. We found that the following three acoustic phenomena occurred, which could be regarded as early signals of rock mass instability: (1) the crackling noises increased significantly; (2) the variation of the b' value exhibited a downward trend; and (3) the effective power-law exponent and the optimal exponent changed in different stages and gradually decreased as the final failure was approached. Furthermore, Figure 5 indicated that the corresponding moment of the b'_1 value occurred significantly earlier than the corresponding time at which the crackling noises significantly increased. Therefore, it was determined that the statistical characteristics of the crackling noise could predict the rock mass failure further in advance than the magnitude of crackling noise could.

Second, the statistical analysis results of the AE energy indirectly proved the presence of self-similarities during the deformation process of the rocks [27, 41–43]. Figure 5 indicated that the change trends of the b' value curves are basically the same. Therefore, it can be seen that the evolution mechanisms of the microfracture activities during the deformation process of the rocks are basically similar. Figure 6 indicated that the change trends of the r' value curves for the two stages of a specimen are also basically

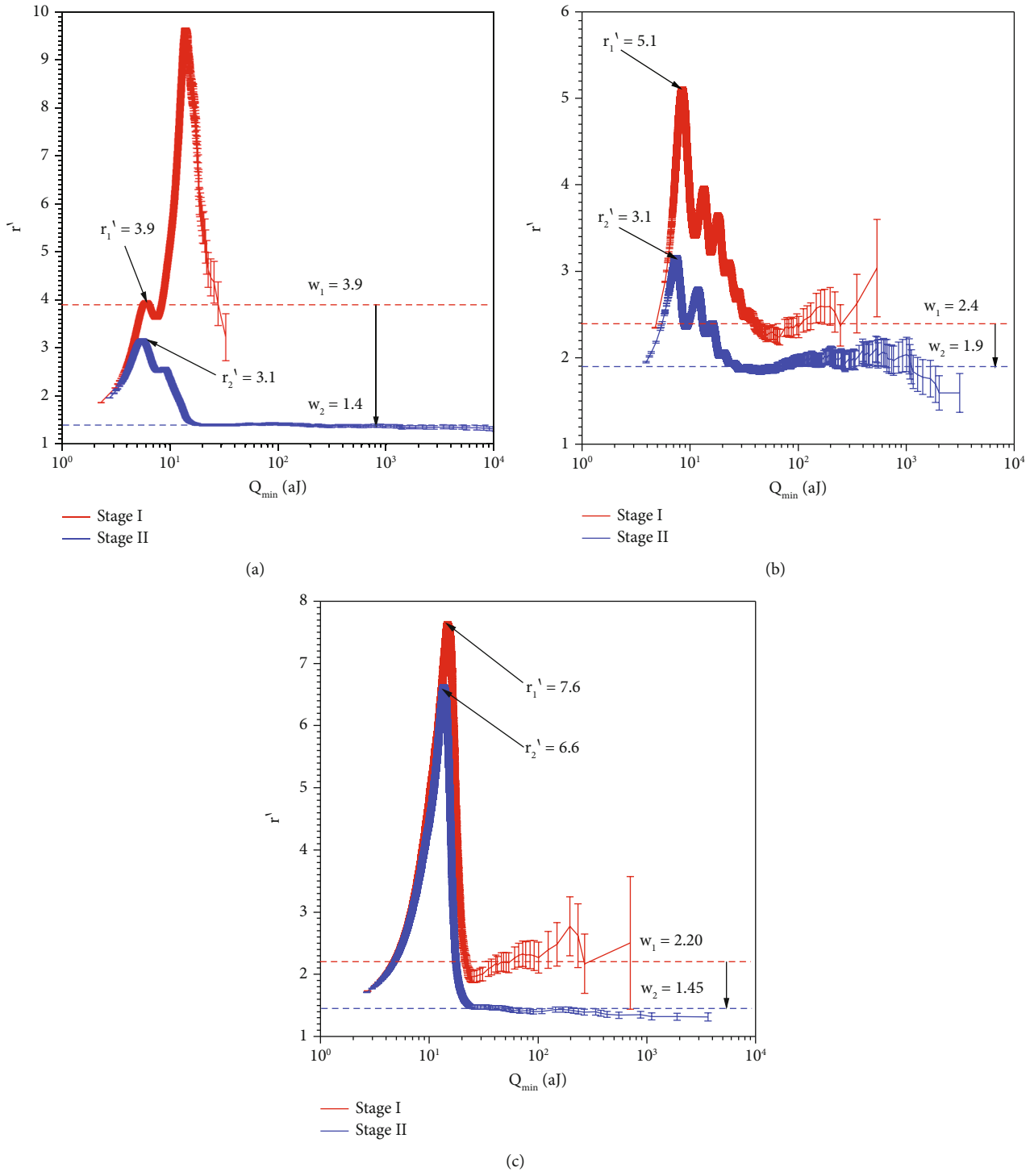

Figure 6: The fitted exponent r' as a function of the lower threshold Q_{min}: (a) A-1, (b) B-1, and (c) C-1. The error bars at each data point show the standard error, and the dotted line defines the value of the optimal exponent.

Table 3: Exponents of selected samples and their difference values.

Specimen	Effective power-law exponent		Optimal exponent	
	Category	Value	Category	Value
A-1	r_1'	3.90	w_1	3.90
	r_2'	3.10	w_2	1.40
	Δr	0.80	Δw	2.50
B-1	r_1'	5.10	w_1	2.40
	r_2'	3.10	w_2	1.90
	Δr	2.00	Δw	0.50
C-1	r_1'	7.60	w_1	2.20
	r_2'	6.60	w_2	1.45
	Δr	1.00	Δw	0.75

the same. Therefore, it can be seen that the microfracture activities for each stage are also basically similar in the statistical distribution. Thus, the statistical analysis results of acoustic emission energy are of considerable significance to further study the self-organized critical behavior of rocks and the fractal dimensions of acoustic emission parameters.

5. Conclusions

In order to further understand the anisotropy behavior and destabilization precursor of layered rocks, a series of uniaxial compression experiments were designed and carried out on layered and intact specimens to study the anisotropic behavior and the statistical evolution of acoustic emission energy during the deformation of layered sandstone. The main conclusions of this paper can be concluded as follows:

(1) The peak strength and elastic modulus of the layered samples were smaller than those of the intact samples; however, there was little difference in the peak strain between the layered specimens and intact specimens. At the same time, the mechanical parameters of the specimens were also affected by the bedding inclination, and the strength of the specimens with large bedding inclination was usually low under uniaxial compression

(2) The failure modes of the selected samples were related to the bedding planes and bedding inclination, and the failure modes of the specimens with a large bedding inclination were usually "layer activation" modes

(3) The variation of the b value showed a significant downward trend, and the acoustic emission energy increased rapidly to the peak values, which were used as "early warning signals" before the final collapse occurred

(4) The power-law exponent of the crackling noises during the rock failure process changed in different stages and gradually decreased as the final failure was approached, which could be regarded as a warning signal for the impending major collapse

Data Availability

The data used to support the findings of this study are included within the article.

Conflicts of Interest

The authors declare no conflict of interest.

Authors' Contributions

Shujian Li and Shaobin Dong conceived and designed the experiments; Shujian Li, Menglai Wang, and Jingguo Luo performed the experiments; Shujian Li, Menglai Wang, and Yanhong Xie analyzed the data; and Shujian Li, Shaobin Dong, and Binting Cai wrote the paper.

Acknowledgments

This study was financially supported by Yunnan Provincial Research Fund for Post-Doctoral Orientation in 2021.

References

[1] P. Berest, B. Brouard, B. Feuga, and M. Karimi-Jafari, "The 1873 collapse of the Saint-Maximilien panel at the Varangeville salt mine," *Journal of Rock Mechanics and Mining Sciences*, vol. 45, no. 7, pp. 1025–1043, 2008.

[2] S. Z. Zhang, G. W. Fan, D. S. Zhang, and Q. Z. Li, "Physical simulation research on evolution laws of clay aquifuge stability during slice mining," *Earth Science*, vol. 77, no. 7, pp. 1–10, 2018.

[3] A. Taliercio and G. S. Landriani, "A failure condition for layered rock," *International Journal of Rock Mechanics and Mining Sciences & Geomechanics Abstracts*, vol. 25, no. 5, pp. 299–305, 1988.

[4] J. H. Ye, F. Q. Wu, and J. Z. Sun, "Estimation of the tensile elastic modulus using Brazilian disc by applying diametrically opposed concentrated loads," *International Journal of Rock Mechanics and Mining Sciences*, vol. 46, no. 3, pp. 568–576, 2009.

[5] A. Tavallali and A. Vervoort, "Effect of layer orientation on the failure of layered sandstone under Brazilian test conditions," *International journal of rock mechanics and mining sciences*, vol. 47, no. 2, pp. 313–322, 2010.

[6] H. Wu, G. Y. Zhao, and S. W. Ma, "Failure behavior of horseshoe-shaped tunnel in hard rock under high stress: phenomenon and mechanisms," *Transactions of Nonferrous Metals Society of China*, vol. 32, no. 2, pp. 639–656, 2022.

[7] P. F. Yin and S. Q. Yang, "Experimental investigation of the strength and failure behavior of layered sandstone under uniaxial compression and Brazilian testing," *Acta Geophysica*, vol. 66, no. 4, pp. 585–605, 2018.

[8] J. M. He and L. O. Afolagboye, "Influence of layer orientation and interlayer bonding force on the mechanical behavior of shale under Brazilian test conditions," *Acta Mechanica Sinica*, vol. 34, no. 2, pp. 349–358, 2018.

[9] G. Khanlari, B. Rafiei, and Y. Abdilor, "An experimental investigation of the Brazilian tensile strength and failure patterns of laminated sandstones," *Rock Mechanics and Rock Engineering*, vol. 48, no. 2, pp. 843–852, 2015.

[10] B. Debecker and A. Vervoort, "Experimental observation of fracture patterns in layered slate," *International Journal of Fracture*, vol. 159, no. 1, pp. 51–62, 2009.

[11] A. Tavallali and A. Vervoort, "Behaviour of layered sandstone under Brazilian test conditions: layer orientation and shape effects," *Journal of Rock Mechanics and Geotechnical Engineering*, vol. 5, no. 5, pp. 366–377, 2013.

[12] A. Vervoort, K. B. Min, H. Konietzky et al., "Failure of transversely isotropic rock under Brazilian test conditions," *International Journal of Rock Mechanics and Mining Sciences*, vol. 70, pp. 343–352, 2014.

[13] Z. G. He, G. S. Li, S. C. Tian, H. Z. Wang, Z. H. Shen, and J. B. Li, "SEM analysis on rock failure mechanism by supercritical CO_2 jet impingement," *Journal of Petroleum Science and Engineering*, vol. 146, pp. 111–120, 2016.

[14] W. Tian and N. V. Han, "Mechanical properties of rock specimens containing pre-existing flaws with 3D printed materials," *Strain*, vol. 53, no. 6, p. e12240, 2017.

[15] Y. H. Huang, S. Q. Yang, and W. L. Tian, "Crack coalescence behavior of sandstone specimen containing two preexisting flaws under different confining pressures," *Theoretical and Applied Fracture Mechanics*, vol. 99, pp. 118–130, 2019.

[16] D. Lockner, "The role of acoustic emission in the study of rock fracture," *International Journal of Rock Mechanics and Mining Sciences & Geomechanics Abstracts*, vol. 30, no. 7, pp. 883–899, 1993.

[17] R. A. Winner, G. Y. Lu, R. Prioul, G. Aidagulov, and A. P. Bunger, "Acoustic emission and kinetic fracture theory for time-dependent breakage of granite," *Fracture Mechanics of Ceramics*, vol. 199, pp. 101–113, 2018.

[18] S. T. Miao, P. Z. Pan, Z. H. Wu, S. J. Li, and S. K. Zhao, "Fracture analysis of sandstone with a single filled flaw under uniaxial compression," *Fracture Mechanics of Ceramics*, vol. 204, pp. 319–343, 2018.

[19] S. Hergarten and H. J. Neugebauer, "Self-organized criticality in a landslide model," *Research Letters*, vol. 25, no. 6, pp. 801–804, 1998.

[20] Y. Ben-Zion, "Collective behavior of earthquakes and faults: continuum-discrete transitions, progressive evolutionary changes, and different dynamic regimes," *Reviews of Geophysics*, vol. 46, no. 4, 2008.

[21] H. Wang, T. H. Yang, and Y. J. Zuo, "Experimental study on acoustic emission of weakly cemented sandstone considering bedding angle," *Shock and Vibration*, vol. 2018, Article ID 6086583, 12 pages, 2018.

[22] S. W. Zhang, K. J. Shou, X. F. Xian, J. P. Zhou, and G. J. Liu, "Fractal characteristics and acoustic emission of anisotropic shale in Brazilian tests," *Tunnelling and Underground Space Technology*, vol. 71, pp. 298–308, 2018.

[23] J. Wang, L. Z. Xie, H. P. Xie et al., "Effect of layer orientation on acoustic emission characteristics of anisotropic shale in Brazilian tests," *Journal of Natural Gas Science and Engineering*, vol. 36, pp. 1120–1129, 2016.

[24] M. V. M. S. Rao and K. J. P. Lakshmi, "Analysis of b-value and improved b-value of acoustic emissions accompanying rock fracture," *Current Science*, vol. 89, pp. 1577–1582, 2005.

[25] J. S. Kim, K. S. Lee, W. J. Cho, H. J. Choi, and G. C. Cho, "A comparative evaluation of stress-strain and acoustic emission methods for quantitative damage assessments of brittle rock," *Rock Mechanics and Rock Engineering*, vol. 48, no. 2, pp. 495–508, 2015.

[26] Q. Zhang and X. P. Zhang, "A numerical study on cracking processes in limestone by the b-value analysis of acoustic emissions," *Computers and Geotechnics*, vol. 92, pp. 1–10, 2017.

[27] E. K. H. Salje, A. Saxena, and A. Planes, "Avalanches in functional materials and geophysics," Springer International Publishing, Cham Switzerland, 2017.

[28] X. G. Kong, E. Y. Wang, S. B. Hu, R. X. Shen, X. L. Li, and T. Q. Zhan, "Fractal characteristics and acoustic emission of coal containing methane in triaxial compression failure," *Journal of Applied Geophysics*, vol. 124, pp. 139–147, 2016.

[29] D. M. Zhang, S. J. Li, X. Bai, Y. S. Yang, and Y. P. Chu, "Experimental study on mechanical properties, energy dissipation characteristics and acoustic emission parameters of compression failure of sandstone specimens containing en echelon flaws," *Applied Sciences*, vol. 9, no. 3, p. 596, 2019.

[30] M. Ohtsu and C. U. Grosse, *Acoustic emission testing*, Springer Science & Business Media, 2008.

[31] B. Gutenberg and C. F. Richter, "Frequency of earthquakes in California," *Bulletin of the Seismological society of America*, vol. 34, no. 4, pp. 185–188, 1944.

[32] S. Akdag, M. Karakus, A. Taheri, G. Nguyen, and M. C. He, "Effects of thermal damage on strain burst mechanism for brittle rocks under true-triaxial loading conditions," *Rock Mechanics and Rock Engineering*, vol. 51, no. 6, pp. 1657–1682, 2018.

[33] Z. L. Ge and Q. Sun, "Acoustic emission (AE) characteristics of granite after heating and cooling cycles," *Fracture Mechanics of Ceramics*, vol. 200, pp. 418–429, 2018.

[34] H. J. Wang, F. Zhao, Z. Q. Huang, H. C. Yu, J. R. Niu, and P. Zhang, "Study on acoustic emission characteristics of sandstone under different fracture modes," *Arabian Journal of Geosciences*, vol. 11, no. 24, p. 772, 2018.

[35] X. Ma, E. Westman, B. Slaker, D. Thibodeau, and D. Counter, "The b-value evolution of mining-induced seismicity and mainshock occurrences at hard-rock mines," *International Journal of Rock Mechanics and Mining Sciences*, vol. 104, pp. 64–70, 2018.

[36] J. Riviere, Z. Lv, P. A. Johnson, and C. Marone, "Evolution of b -value during the seismic cycle: Insights from laboratory experiments on simulated faults," *Science Letters*, vol. 482, pp. 407–413, 2018.

[37] Y. J. Tan, F. Waldhauser, M. Tolstoy, and W. S. D. Wilcock, "Axial Seamount: periodic tidal loading reveals stress dependence of the earthquake size distribution (b value)," *Science Letters*, vol. 512, pp. 39–45, 2019.

[38] P. Datt, J. C. Kapil, and A. Kumar, "Acoustic emission characteristics and b-value estimate in relation to waveform analysis for damage response of snow," *Cold Regions Science and Technology*, vol. 119, pp. 170–182, 2015.

[39] T. Utsu, "Representation and analysis of the earthquake size distribution: a historical review and some new approaches," in *Pure and Applied Geophysics*, vol. 155, no. 2-4, pp. 509–535, 1999.

[40] H. Li, X. C. Yin, S. Y. Li, and J. H. Li, "The experimental research onb value of AE for the rock specimens with preexisting crack or notch under uniaxial compression," *Acta Seismologica Sinica*, vol. 5, no. 4, pp. 867–875, 1992.

[41] T. Hirata, T. Satoh, and K. Ito, "Fractal structure of spatial distribution of microfracturing in rock," *Geophysical Journal International*, vol. 90, no. 2, pp. 369–374, 1987.

[42] C. G. Hatton, I. G. Main, and P. G. Meredith, "A comparison of seismic and structural measurements of scaling exponents during tensile subcritical crack growth," *Journal of Structural Geology*, vol. 15, no. 12, pp. 1485–1495, 1993.

[43] E. K. H. Salje, X. Jiang, J. Eckstein, and L. Wang, "Acoustic emission spectroscopy: applications in geomaterials and related materials," *Applied Sciences*, vol. 11, no. 19, p. 8801, 2021.